

the clad region of the fibre was fully immersed in turn in a range of pH buffer solutions from a pH of 2 to 8. Fig. 3 shows the fluorescence intensity at  $\lambda = 530$  nm, recorded as a function of pH, for a fixed laser emission power of 3 mW. It can be

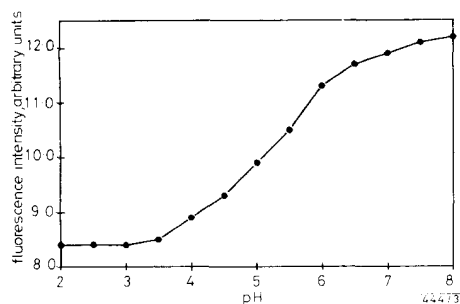


Fig. 3 pH sensitivity of sol-gel sensor

seen that greatest sensitivity to pH change occurs in the region pH 3.5–6.5. The response time of the sensor to a step change in pH was found to be approximately 5 s. This time appears to be governed by the mass transfer of the hydrogen ions through the sol-gel matrix to the fluorescein molecules. Although higher signals could be achieved by increasing the laser power, significant photobleaching of the dye became evident. Finally, no washout of the dye was observed as the fluorescent intensity in water remained constant despite repeated washings.

**Conclusion:** The use of porous sol-gel glass as a support structure for chemically-sensitive dyes in evanescent-wave optical waveguide sensors has been demonstrated. The low temperature of the process enables use of a wide range of dyes of low thermal stability. This novel technique is particularly suited to gas sensing where the high specific area of the continuous porous structure is particularly important. In addition, it offers the potential for fully distributed or quasidistributed multipoint sensing. This could be achieved by coating a fibre along its total length during drawing or by splicing in sensing regions. Where simple point sensing is required, it is a relatively straightforward process to coat the endface of a fully clad fibre. Finally, the compatibility of the sol-gel coating with the silica substrate makes the technique particularly suitable for planar waveguide sensors formed by ion exchange in glass.

B. D. MCCRAITH  
V. RUDDY  
C. POTTER  
School of Physical Sciences  
Dublin City University  
Glasnevin, Dublin 9, Ireland

B. O'KELLY  
J. F. MCGILP

Department of Pure and Applied Physics  
Dublin University  
Trinity College  
Dublin 2, Ireland

#### References

- NORRIS, J. O. W.: 'Current status and prospects for the use of optical fibres in chemical analysis—a review', *Analyst*, 1989, **114**, pp. 1359–1372
- LIEBERMAN, R. A., BLYLER, L. L., and COHEN, L. G.: 'A distributed fiber-optic sensor based on cladding fluorescence', *J. Lightwave Technol.*, 1990, **8**, (2), pp. 212–220
- WOLFBES, O. S.: 'Fibre optical fluorosensors in analytical and clinical chemistry', in SCHULMAN, S. J. (Ed.): 'Molecular luminescence spectroscopy—Part II' (John Wiley & Sons, New York, 1988), pp. 129–281
- MUKHERJEE, S. P.: 'Sol-gel processes in glass science and technology', *J. Non-Cryst. Solids*, 1980, **42**, pp. 477–488
- FUH, M. S., BURGESS, L. W., HIRSCHFELD, T., CHRISTIAN, G. D., and WANG, F.: 'Single fibre optic fluorescence pH probe', *Analyst*, 1987, **112**, pp. 1159–1163

1248

## BiCMOS EDGE DETECTOR WITH CORRELATED-DOUBLE-SAMPLING READOUT CIRCUIT FOR PATTERN RECOGNITION NEURAL NETWORK

Indexing terms: Detectors and detector circuits, Image processing, Neural networks

A new image sensor is presented that comprises a chopper-stabilised edge detector and a correlated-double-sampling readout circuit, based on  $2\mu\text{m}$  BiCMOS technology for pattern recognition neural network VLSI applications operating at 77 K. With the chopper-stabilised edge detector and the correlated-double-sampling readout technique, the two-dimensional photodiode array, which can be efficiently built with only one readout circuit, provides a bidirectional edge detection capability for high resolution image sensing applications operating at 77 K.

**Introduction:** Recently, pattern recognition implemented by the neural network techniques has been the major method for machine vision applications. Usually, the image of the object is recorded by a 2-D photodetector array such as charge-coupled device (CCD), followed by the edge detection of the object; the recognition function is then performed. A 'smart' edge detector resembling the response of a biological retina, which is made of over 30 transistors and one phototransistor as a pixel unit and can be used to extract the edge position of an object image, has been realised using CMOS analogue VLSI circuit techniques.<sup>1</sup> A simpler 'off-centre' edge detector composed of two back-to-back-connected concentric or directional photodiodes realised by amorphous silicon technology has also been reported.<sup>2</sup> The generated edge signal, which can be either positive or negative, is proportional to the difference of the two photocurrents associated with two photodiodes if the edge of the image happens to fall on the detector. In this Letter, a new image sensor using two pairs of cross-coupled BiCMOS photodiodes with chopper-stabilised switches and a correlated-double-sampling readout circuit operating at 77 K for bidirectional edge detection, is described.

**Edge detector circuit:** This new image-sensor is composed of an edge detector array and a readout circuit. As shown in Fig. 1 in each pixel area, two cross-coupled pairs of back-to-back-connected photodiodes can be used to perform bidirectional edge detection. Compared with traditional image sensors such

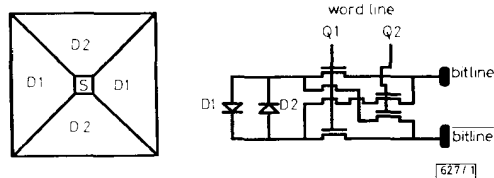


Fig. 1 Cross-coupled pairs of back-to-back-connected photodiodes in each pixel area

as CCDs, in the edge detector each pair of photodiodes generates a nonzero net current only when an image edge falls on the detector. This arrangement facilitates an efficient recording of the edge information of an image. The readout circuit comprises a word-line decoder, a bit-line decoder, and a current integrator/output buffer. As in SRAM memory cells, together with the word-line and bit-line decoder outputs, four-pass transistors using chopper-stabilised techniques<sup>3</sup> are used to provide access to the current integrator/output buffer for each individual pair of the photodiodes as shown in Fig. 2. In addition, the chopper-stabilised switches also facilitate bidirectional edge detection as a result of the nonzero net current coming from the photodiode pair. Consequently, a two-dimensional edge detector array can be constructed with the basic edge detector cell, which is composed of two cross-coupled pairs of back-to-back-connected photodiodes and eight switches. Furthermore, only one readout circuit is necessary for the whole edge detector array and the effective area in

image sensing can be raised owing to the drastic reduction of the nonphotodiode area. As shown in Fig. 2, the current

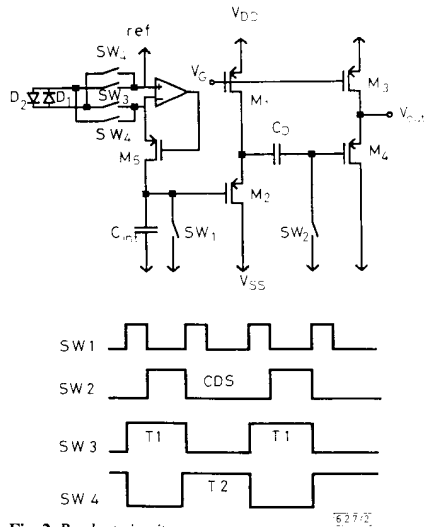


Fig. 2 Readout circuit

integrator/output buffer, which is used to convert the photocurrent into an output voltage signal for further processing is made of an opamp, an integrating capacitor  $C_{int}$ , a reset switch SW1, and a feedback  $p$ MOS transistor to ensure a zero-biased operation for the accessed photodiodes at an optimised efficiency. Two  $p$ MOS source followers with a capacitor  $C_D$ , and a switch SW2 are used as an output buffer with a correlated-double-sampling mechanism<sup>4</sup> to reduce noise effects and to facilitate recording of the nonzero net current from the photodiodes with clock timing as shown. During T1, SW3s are on and the selected photodiodes are connected to the readout circuit. As SW1 is high, the integrating capacitor  $C_{int}$  is grounded and capacitor  $C_D$  is floating. As SW2 turns on and SW1 is off, integrating capacitor  $C_{int}$  is charged by the photocurrent generated by the accessed photodiodes, and the right plate of the capacitor  $C_D$  is grounded. At the end of the T1 period, the capacitor  $C_D$  contains the sampled reset noise and the charge associated with the photocurrent of the same photodiodes biased at a polarity set by SW3s. During T2, the polarity of the selected photodiodes is reversed and SW2 is always off. As SW1 turns off, the charge corresponding to the photocurrent of the same photodiodes with the polarity reversed by turning on SW4s is coupled to capacitor  $C_D$ . The difference in charge associated with capacitor  $C_D$  between T1 and T2 shows up in the output voltage  $V_{out}$  at the end of the T2 period. Incorporating the modified correlated-double-sampling mechanism, the new detector circuit not only can detect a positive or negative photocurrent but also can reduce the thermal and flicker noise effects generated in the analogue front end of the readout circuit.

**Circuit performance:** CMOS analogue circuits operating at 77 K offer low noise advantages,<sup>5</sup> which are particularly important for high performance image sensing circuits.<sup>6</sup> Currently, SPICE device models are not sufficient for simulation of circuits operating at 77 K. To design the image sensor operating at 77 K, low temperature SPICE models have been successfully developed. With appropriate low temperature models, a CMOS two-stage opamp with a DC gain of over 1000, and a unity gain bandwidth of 2 MHz has been designed. Overall transient behaviour of the image sensing circuit operating at 77 K is shown in Fig. 3.

In a pixel area, with photodiode D2 illuminated by a light source and the other photodiode, D1, masked, the output voltage  $V_{out}$  actually shows a larger value at the end of T2 as compared to that at the end of T1. On the other hand, with D2 masked and D1 illuminated, a smaller output voltage at the end of T2 can be seen. Experimental low temperature

results confirm the simulation results as shown. Thus, the bidirectional edge detection capability of the new image sensing circuit using a chopper-stabilised edge detector and a correlated-double-sampling readout circuit has been verified. Fig. 4 shows the layout of the  $2 \times 2$  image sensing circuit based on  $2 \mu\text{m}$  BiCMOS technology. Digital bit-line and word-line decoder circuits are shown in the upper and central portions of the figure. The centre-right portion is the edge detector array and at lower right is the opamp related readout circuit. Total chip area is around  $1400 \mu\text{m} \times 1200 \mu\text{m}$ .

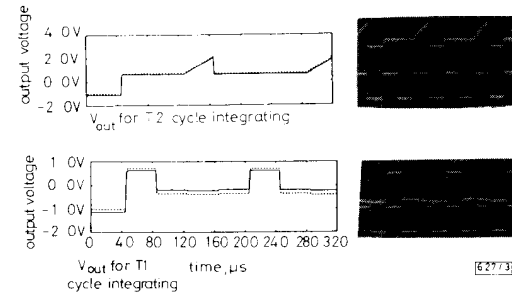


Fig. 3 Overall transient behaviour of image sensing circuit operating at 77 K

--- temperature = 25.0°C  
— temperature = -196.0°C

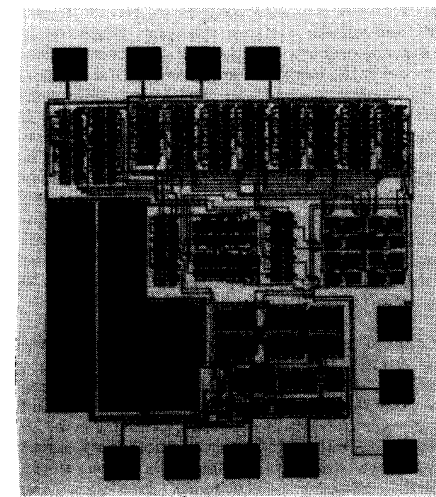


Fig. 4 Layout of image sensing circuit

**Conclusion:** In conclusion, with the chopper-stabilised edge detector and the correlated-double-sampling readout circuit, the new sensing circuit can provide an SRAM-type two-dimensional expansion capability in implementing pattern recognition VLSI for bidirectional edge detection at 77 K.

J. B. KUO  
T. L. CHOU  
E. J. WONG  
22nd April 1991  
Rm. 526  
Department of Electrical Engineering  
National Taiwan University  
Roosevelt Rd.  
Sec. 4, Taipei 107, Taiwan, Republic of China

#### References

- MEAD, C.: 'Analog VLSI and neural systems' (Addison Wesley, 1989)
- SAH, W. J., LEE, S. C., and CHEN, J. H.: 'Amorphous silicon edge detector for application to electronic eyes'. IEEE Dig. of Int. Electron Device Meeting, December 1989, pp. 515-518

- 3 HSIEH, K. C., GRAY, P. R., SENDEROWICZ, D., and MESSERSCHMITT, D. G.: 'A low-noise chopper-stabilized switched-capacitor filtering technique', *IEEE J. Solid-State Circuits*, 1981, **SC-16**, (6), pp. 708-715
- 4 KANSY, R. J.: 'Response of a correlated double sampling circuit to 1/f noise', *IEEE J. Solid-State Circuits*, 1980, **SC-15**, (3), pp. 373-375
- 5 FOX, R. M., and JAEGER, R. C.: 'MOSFET behavior and circuit consideration for analog applications at 77 K', *IEEE Trans.*, 1987, **ED-34**, (1), pp. 114-123
- 6 SCHOENEKER, U., HOSTICKA, B. J., FENT, J., OBERLACK, H., and ZIMMER, G.: 'CMOS readout electronics for operating at cryogenic temperatures', *IEEE J. Solid-State Circuits*, 1989, **SC-24**, (3), pp. 718-722

## FIELD TRIAL EVALUATION OF LINEAR MODULATION SINGLE SIDEBAND

*Indexing terms: Radiocommunication, Mobile radio systems*

A series of field trials to assess the performance of a VHF trunked PMR system using 5 kHz bandwidth linear modulation single sideband technology compared with existing 12.5 kHz FM and AM systems are described. Relative performance figures are given.

**Introduction:** With the ever increasing use of private mobile radio (PMR) and cellular systems, spectrum congestion is becoming a pressing problem. One possible step towards effective spectrum use is the introduction of narrowband systems, such as 5 kHz channel spaced linear modulation single sideband (LM-SSB). To provide information on the effects of such an introduction, the DTI Radiocommunications Agency commissioned Bradford University to carry out a series of independent field trials to compare the performance of 5 kHz LM-SSB with 12.5 kHz FM and AM, operating between 165 and 170 MHz. The LM-SSB system under test was a prototype model using the transparent tone in band (TTIB) technique developed at Bristol University.<sup>1</sup> This prototype model was compared with a Tait T377 FM system with two T530 mobiles and a Pye T401 AM system with M201 mobiles.

**Field trial implementation:** Measurements were made for transmissions from a base station to a mobile following a carefully defined route at a constant 30 mph. Each base station was calibrated to give equal average incident field strength. Both voice and data measurements were taken for all three modulation schemes without interference, and a subset of these experiments was then repeated with various single, voice-modulated, adjacent or cochannel interferers. The channel separation for adjacent channel tests was 5 kHz for two SSB channels, and 10 kHz for other cases. The results given here are for a composite route made up of individual sections with average signal strength ranging from 52 dB  $\mu$ V to under 0 dB  $\mu$ V and widely varying fading depths. The only exception to this is the cochannel results which are carried out on a single route of signal strength between 10 dB  $\mu$ V and 36 dB  $\mu$ V and fading greater than 10 dB. The methods of assessment used were as follows:

- (1) The speech intelligibility of the systems was investigated using the diagnostic rhyme test (DRT),<sup>2</sup> which uses a panel of listeners to produce a score for average percentage unintelligibility. Listeners also scored each entire test on a five point scale, to include some element of subjective quality assessment.
- (2) The bit error rate (BER) was used as a measure of the ability of the systems to transmit data. V23, V27bis and V29 modems were used to measure the BER for data rates between 1.2 Kbit/s and 9.6 Kbit/s.

**Voice results:** Fig. 1 shows the percentage unintelligibility scores for SSB, FM and AM with no interference and with

adjacent channel interference. From the baseline performance measurements, it can be seen that SSB performs significantly

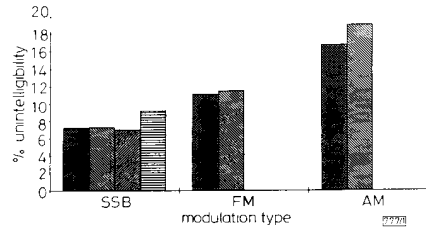


**Fig. 1** Voice results with adjacent channel interference

Composite route  
 ■ baseline      ■ SSB interference  
 ■ FM interference      ■ AM interference

better than either FM or AM. However, despite its high objective intelligibility, SSB proved unpopular with listeners, who found its tone unpleasant.

In terms of interference, SSB is highly resistant to both SSB and FM adjacent channel interference. However, AM interference has a significant effect on SSB, and this is likely to be the limiting factor in the integration of SSB with an existing spectral environment. It is interesting to note that LM-SSB with any form of interference performs better than baseline FM or AM.

As previously stated, cochannel measurements were taken for each system on one sample route (rather than the composite route). Two protection ratios, of 2 dB and 8 dB, were used, and with the results obtained, estimates for the required protection ratios for two different scenarios were made for each of the channel configurations tested.

- (1) The value of protection ratio required to obtain a DRT intelligibility score identical to the relevant baseline measurement was calculated. This is the protection ratio required for the interferer to have no noticeable effect on the speech intelligibility.
- (2) Also calculated was the value of protection ratio required to give a chosen DRT figure of 10% unintelligibility, assessed by the listeners as 'tolerable'.

For both of these protection ratio figures, a linear relationship between the intelligibility and protection ratio is assumed. Table 1 shows the calculated protection ratios. It can be seen

**Table 1** ESTIMATED PROTECTION RATIOS FOR VOICE WITH COCHANNEL INTERFERENCE

|     | SSB interference |      | FM interference |      | AM interference |      |
|-----|------------------|------|-----------------|------|-----------------|------|
|     | NE               | 10%  | NE              | 10%  | NE              | 10%  |
| SSB | 12.0             | 6.5  | 17.5            | 11.5 | 23.5            | 10.0 |
| FM  | 24.0             | 20.0 |                 |      |                 |      |
| AM  | 10.0             | —    |                 |      |                 |      |

NE: Protection ratio for no effect on intelligibility

10%: Protection ratio for 10% unintelligibility

that FM is extremely susceptible to SSB cochannel interference but that AM is fairly resistant. SSB is highly resistant to SSB interference, less so to FM interference and is badly affected by AM. However, the 10% protection ratios for all these positions are low because of the good absolute intelligibility of SSB.

**Data results:** Fig. 2 shows the number of errors per million bits for the three modulation schemes; a variety of bit rates using various baseband modems are used for SSB and FM, but not for AM. This figure shows the difficulty that this implementation of LM-SSB has in coping with data rates above 2.4 Kbit/s using standard line modems. Fig. 3 shows the effects of voice modulated adjacent channel interference on 1.2 Kbit/s data transmission. In all cases, the effect is much